Journal Pre-proof

Investigating the intracellular bactericidal effects of rifampicin loaded S-protected thiomeric chitosan nanocargoes against *Mycobacterium tuberculosis*

Aisha Rauf, Sobia Razzaq, Tanveer A. Tabish, Sabira Tahseen, Mansoor Abdullah Sandhu, Gul Shahnaz

Please cite this article as: A. Rauf, S. Razzaq, T.A. Tabish, S. Tahseen, M.A. Sandhu, G. Shahnaz, Investigating the intracellular bactericidal effects of Rifampicin loaded S-protected thiomeric chitosan nanocargoes against *Mycobacterium tuberculosis*, *Journal of Drug Delivery Science and Technology*, https://doi.org/10.1016/j.jddst.2020.102184.

This is a PDF file of an article that has undergone enhancements after acceptance, such as the addition of a cover page and metadata, and formatting for readability, but it is not yet the definitive version of record. This version will undergo additional copyediting, typesetting and review before it is published in its final form, but we are providing this version to give early visibility of the article. Please note that, during the production process, errors may be discovered which could affect the content, and all legal disclaimers that apply to the journal pertain.

Aisha Rauf: Conceptualization, investigation, methodology, software, writing and editing; **Sobia Razzaq:** Software, analysis; **Tanveer A Tabish:** Reviewing and editing; **Sabira Tahseen:** Supervision, Resources, Validation; **Mansoor Abdullah Sandhu:** Resources, validation, investigation, formal analysis; **Gul Shahnaz:** Supervision, methodology, writing-reviewing and editing.

Graphical abstract

1
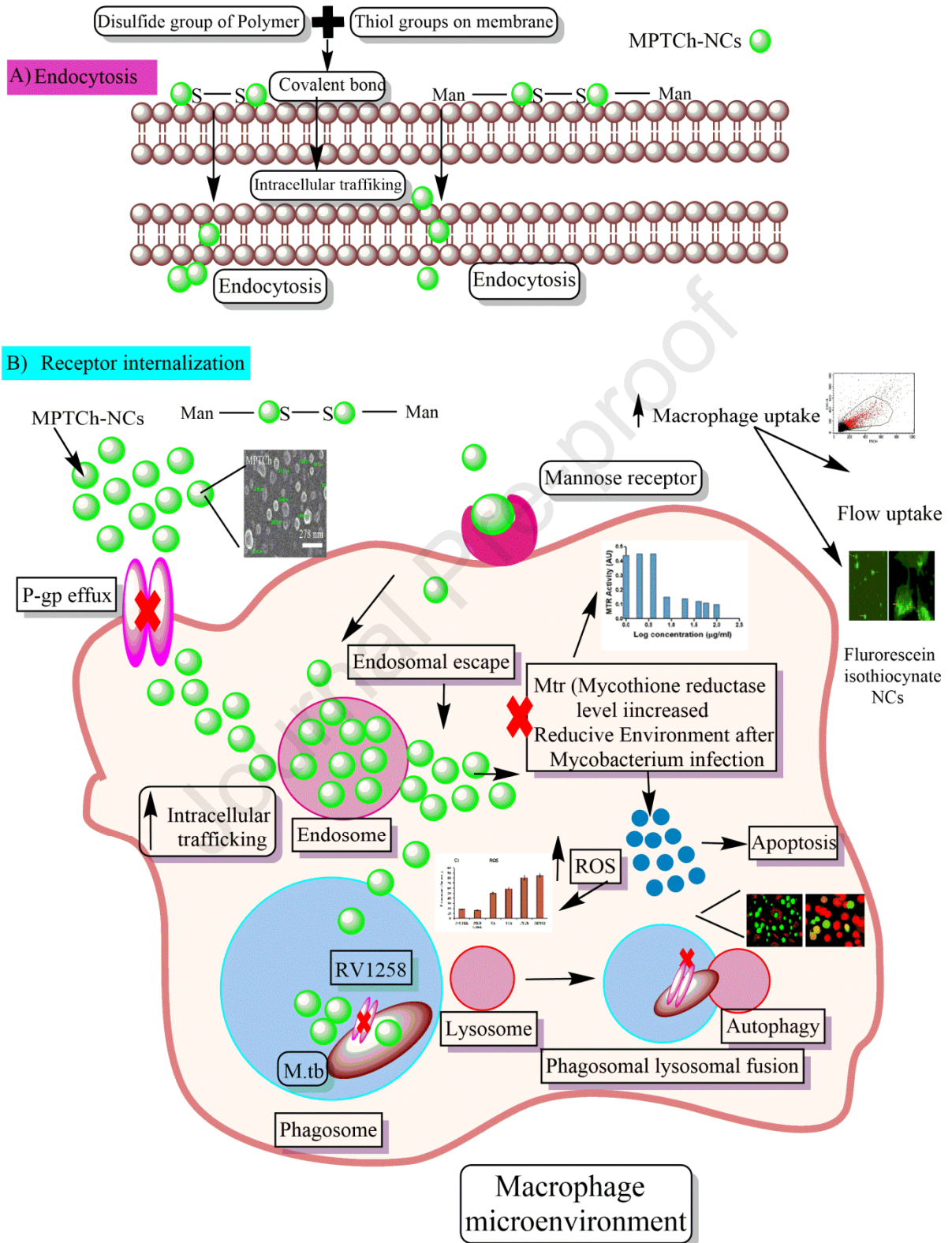
1 **Investigating the intracellular bactericidal effects of Rifampicin loaded S-protected**

2 **thiomeric chitosan nanocargoes against *Mycobacterium tuberculosis***

3 Aisha Rauf[a], Sobia Razzaq[a], Tanveer A. Tabish[b], Sabira Tahseen[c], Mansoor Abdullah Sandhu[d],

4 and Gul Shahnaz[a*]

5 [a] Department of Pharmacy, Faculty of Biological Sciences, Quaid-i-Azam University, Islamabad,

6 45320, Pakistan.

7 [b]UCL Cancer Institute, University College London, London, WC1E 6DD, UK

8 [c]National Technical Advisor (NRL) National TB Control Programme Pakistan

9 [d]Department of Biomedical Sciences, Faculty of Veterinary and Animal Sciences, PMAS-Arid

10 Agriculture University, Rawalpindi Pakistan.

11 ***Correspondence**

12 **Gul Shahnaz**

13 Department of Pharmacy, Faculty of Biological Sciences, Quaid-i-Azam University, Islamabad,

14 45320, Pakistan. Email: gshshnaz@qau.edu.pk

15 Tel.: +92 51 90644137

16

17

18

19

20

21

22

Abstract

The antibiotic drug resistance in *Mycobacterium tuberculosis* (M.tb) is typically associated with immune evasion shared by pathogenic bacterium and intrinsic antimycobacterial drug resistance. These factors significantly contribute to the limited delivery of drugs intracelullary thereby posing an ever-growing threat to mankind. A promising approach to tackle this multi-drug resistance is to use nanocargoes (NCs) based drug delivery approach. The aim of the present study was to develop mannose coated S-protected thiomeric site-specific nanocargoes (MPTCh-NCs) of Rifampicin (Rif) in order to deliver drug locally inside the macrophages. This NCs-based delivery system modifies the macrophage activation states *via* mannose receptors and endocytosis to alter the macrophage activation state thus providing synergistic antimycobacterial effects. MPTCh-NCs were synthesized by ionic gelation method and assessed for particle size and encapsulation efficiency Moreover, MPTCh-NCs were also investigated in *in vitro* for drug release, macrophage uptake, buffering potential, Mycothione reductase (MTR) inhibition ability, inhibitor concentration (MIC) , phagolysosomal fusion, reactive oxygen species (ROS) production apoptosis and RV 1258 inhibition. The *in vivo* bioavailability study of MPTCh-NCs was also evaluated in male BALB/c models over a period of 72 h. The optimized MPTCh-NC formulation was nanosized (390 $\pm$ 20 nm) with better EE of Rif i.e. 73.68 $\pm$ 5.99 %. The MPTCh-NCs showed better buffering capacity at different pH ranges, 35.69 folds higher macrophage uptake than Rif with P-gp inhibition potential and pronounced MTR inhibition potential. The MPTCh-NCs exhibited MIC of 16 µg/ml by drug susceptibility testing. Flow cytometric analysis of MPTCh-NCs exhibited, increased apoptosis (33.29 %). Real time PCR data suggested enhanced RV 1258 inhibition potential (0.387 fold expression) of the MPTCh-NCs. *In vivo* results indicated increased bioavailability of MPTCh-NCs (AUC 12.31 folds higher) in comparison to conventional drug Rif. In summary, the observed capacity of the mannose coated S-protected NCs-based approach to deliver therapeutic levels of Rif selectively has potential to improve the therapeutic management against drug resistant tuberculosis.

Key words: multidrug resistance, nanocargoes, anti oxidant potential, Mycothione reductase, alternative activation state, S-protected chitosan

1. Introduction

52

53   Tuberculosis (TB) is the deadliest infectious disease with two million deaths annually across the

54   globe. Despite efforts to mitigate its toll on humanity, it is still considered a major threat to

55   public health. The microenvironment conditions and lesions of TB are highly complex and

56   induce diverging trajectories of these lesions within the host's innate immune system. The

57   microenvironment complexity is due to the multiple types of lesions associated with

58   *Mycobacterium tuberculosis* (M.tb). TB microenvironment not only initiates a plethora of

59   immune evasion but also in parallel, provides a niche for *Mycobacterium* survival [1, 2]. The

60   host's immune system limits the mycobacterial spread through a series of events induced by

61   immune system. One of the major limitations of the existing therapeutic modalities is the intra-

62   macrophage localization of the *Mycobacterium*. The p-glycoprotein efflux pumps (EPs) existing

63   on the surface of macrophages is involved in the rapid efflux of certain drugs such as

64   Rifampicin, moxifloxacin, isoniazid and bedaquiline [3]. Additionally, endosomal encapsulation

65   of the drug results both in drug deterioration [4] and in phagolysosomal fusion [5]. The ability of

66   *Mycobacterium* to circumvent the macrophage induced ROS depends on the reduction of

67   mycothiol (MSH). . Enzymes involved in the MSH biosynthesis are considered to be essential

68   for the growth of M.tb. Mycothione Reductase (MTR) is one of these enzymes, which actively

69   participates in M.tb growth. MSH is being converted into its oxidized form such asMSSM as a

70   result of its exposure to ROS. In order to maintain this reducing potential, MTR also catalyzes

71   MSSM and forms MSH. Moreover, MSH plays a pivotal role in *Mycobacterium* survival[6].

72   *Mycobacterium* has EPs existing on its surface which are actively involved in the expulsion of

73   drugs (such as RV1258 for Rif) which in turn diminishes the intracellular drug concentrations.

74   Such strategies mediated by *Mycobacterium* facilitate the reduced intracellular drug levels and

75   subversion of immune response thereby producing the alternative pathways for the activation of

76   macrophages [3, 7].

77   There is an urgent need to develop a drug delivery platform that addresses aforementioned

78   challenges to improve intracellular trafficking, subvert the immune response and to facilitate

79   synergistic bactericidal effects. Different studies have shown that the alternative activation state

80   of macrophages results in the deprivation of coordinated defense systems of M.tb [8].

81   Nanotechnology has gained much attention owing to their tunable shape and size-dependent

82   physiochemical features. NP-based cargo systems (known as nanocargoes) advance the

83   therapeutic and pharmacological performance of chemotherapeutic agents *via* targeted delivery

84   and controlled drug release. This targeted and controlled drug release eliminate the problems

85   associated with conventional drugs such non-selectivity and uncontrolled/unpredictable release

86   [9]. Several nanotechnology-based drug delivery strategies have been developed in order to

87   obtain macrophage activation. For instance, Pi et al., reported that the phagocytosis of the

88   Selenium-nanoparticles (NPs) increased the phagolysosomal destruction of macrophages and

89   enhanced the ROS-mediated programmed cell death [10]. In another study, it has been

90   demonstrated that the phagocytic uptake of glucan-NPs of Rifabutin resulted in the activation of

91   cascade responses within infected macrophages. These responses included enhanced ROS

92   generation, apoptosis and phagolysosomal destruction of the *Mycobacterium* [5]. Therefore,

93   NPs-based delivery formats have emerged as a promising candidate in drug delivery

94   applications. In these regards, a nanocargo (NCs) is a promising solution owing to their high

95   abilities of carrying drugs and releases them selectively (where the drug release is the most

96   needed). Successful delivery of NCs into the cytoplasm of cells involve three critical steps: 1)

97   cellular internalization and localization; 2) stimulation of endocytosis and 3) facilitation of

98   endosomal escape [11]. S-protected thiolated polymers (also known as thiomers comprising thiol

99   groups covalently attached to their backbones) have widely been studied for their increased

100   cellular uptake, efflux pump, enzyme inhibition and permeation enhancing features [12].

101   In this work, we developed a smart, site-specific, S-protected thiomeric chitosan NCs coated

102   with mannose in order to increase the intracellular drug trafficking *via* two ways. Firstly this

103   thiomeric drug delivery platform containing disulfide bonds at the surface of the polymer enables

104   NCs to pass through the cell membrane. by endocytosis entry pathways [11]. Secondly, mannose

105   receptor internalization facilitates the carrier system (MPTCh-NCs) to pass through the

106   macrophage. As prepared NCs were characterized to investigate their increased intracellular drug

107   uptake, P-gp EP inhibition, endosomal escape potential, MTR inhibition and enhanced reactive

108   nitrogen species (RNS) & ROS-mediated cell deaths. The MPTCh-NCs were also evaluated for

109   enhanced phagolysosomal fusion, decreased MIC, inhibition of RV1258 EP and increased

110   bioavailability *in vivo* . Thus we report the mannose coated S-protected thiolated nanocarriers

111   (MPTCh-NCs) with enhanced drug targeting intracellularly while altering the immune escape

112 strategies of *Mycobacterium* thus increasing the pathogen insult via synergistic mycobacterial
113 effect.

2. Materials and Methods

2.1. Chemicals and reagents

116 Chitosan (50,000 Da) with the degree of deacetylation 75-85 %, mercapto nicotinic acid, sodium
117 tripolyphosphate (TPP), thioglycolic acid (TGA) and D-mannose were purchased from Sigma-
118 Aldrich, Germany. Hydroxylamine, 1-ethyl-3-3(3-dimethyl aminopropyl carbodiimide
119 hydrochloride (EDAC), Ellman's reagent and sodium *cyanoborohydride* were purchased from
120 Merck, Germany. Ascorbic acid and dimethyl sulfoxide (DMSO) were purchased from Merck,
121 Pakistan. Penicillin, Streptomycin and RPMI were purchased from Merck, Pakistan. 3-(4,5-
122 dimethylthiazol-2-yl)-2,5-diphenyltetrazolium bromide (MTT) was purchased from Merck,
123 Germany. Rifampicin was given as gift form Pfizer Laboratories Ltd. All solvents used were of
124 HPLC and analytical grade. All the chemical reagents and solutions were used without any
125 further modifications.

2.2. Synthesis of polymeric carrier and basic characterization of nanocargoes

127 The detailed methodology of synthesis of thiolated chitosan, quantification of thiol, mercapto
128 nicotinic acid, mannose and disulfide linkage, H^1NMR (nuclear magnetic resonance), fourier
129 transform infrared (FTIR), differential scanning calorimetry (DSC) and thermogravimetric
130 analysis (TGA) are given in supplementary information section.

2.2.1. Formulation optimization by design expert

132 For the optimized synthesis of nanocargoes Design Expert® software was utilized to optimize the
133 ratio of different ingredients i.e. conjugated polymers (Ch, TCh, PTCh and MPTCh), and
134 tripolyphosphate (TPP) using the central composite design (CCD) The optimization was carried
135 out in terms of particles size, zeta potential, polydispersity index (PDI) and entrapment efficacy
136 (EE) as dependent variables. The matrix generated by the software was used to prepare the actual
137 formulations and analyzed statistically, including linear regression and response surface analysis.
138 Data with p-value < 0.05 was considered significant and included in the model. Based on better
139 fit (including probability F-value, adjusted R-square, noise level, adequate precision and lack of
140 fit F value), the best mathematical model was chosen for each response.

141   NCs were formulated by ionotropic gelation as reported previously, using the optimized ratios

142   suggested by the Design expert®. [13, 14] Blank NCs were prepared by dissolving the polymer

143   (0.2%) in deionized water and TPP (0.2 %) was added dropwise until the appearance of opaque

144   color. For the preparation of enveloped nanocargoes, 0.2% solution of conjugated polymers

145   (Chitosan=Ch, thiolated chitosan=TCh, S-protected thiolated chitosan=PTCh, and mannose-

146   grafted S-protected thiolated chitosan=MPTCh) in 1% (v/v) acetic acid (pH 4.0). and 0.2% TPP

147   solution in deionized water was prepared separately. The specified amount (1mg/ml) of

148   Rifampicin (Rif) was dissolved in DMSO and diluted with the PBS (pH 4.0). The Rif solution

149   was added to the TPP solution and added drop wise to the polymer solution until the appearance

150   of translucent color. The resultant suspension was centrifuged at 13,500 rpm for 30 min and the

151   pellet of NC was collected and re-dispersed in 3% trehalose solution, freeze-dried and stored at

152   4°C [13, 14]

153   *2.2.2. Basic characterization of NCs*

154   Drug-loaded nanocargoes and blank nanocargoes were analyzed for particle size, zeta potential

155   and polydispersity index (PDI) using Nanozeta sizer (Malvern, UK) by diluting the samples 10

156   times so that the electrophoretic mobility of nanocargoes should not be compromised by the

157   aggregation [15].

158   The surface morphology was analyzed using scanning electron microscopy (SEM) (FEI Nova

159   NanoSEM 450, USA). Samples for SEM images were carefully prepared by slow evaporation of

160   a single dilute drop of formulation on carbon-coated copper grid followed by blotting with a drop

161   of 1% ammonium molybdate solution. For better contrast, the dried sample was further coated

162   with gold, using sputter coater (Denton, Desk V HP) operating at 40 mA for 15 sec under

163   vacuum [14].

164   The encapsulation efficiency (EE) of Rif was measured by the indirect method [16] The

165   suspensions of prepared nanocargoes were centrifuged (14,000 g) for 15 min and supernatant

166   was collected [17]. The supernatant was analyzed, using the HPLC method described above, for

167   the quantification of Rif. The encapsulation efficiency was calculated by the formula:

168

169
$$EE \ (\%) = \frac{Amount \ of \ drug \ in \ formulation}{total \ amount \ of \ drug \ added} \times 100\%)$$

170 ### *2.2.3. In vitro drug release*

171 *In vitro* drug release profile of the polymeric (Ch, TCh, PTCh, and MPTCh) NC was studied at

172 physiological pH i.e. 7.4 (PBS) and macrophage endosomal pH 5.5 (PBS) by using the dialysis

173 tube technique. Briefly, NC suspension equivalent to 10 mg of Rif was taken in the dialysis tube

174 (MW cut off =12-14 kDa) and suspended in the beaker containing the dissolution medium of

175 50ml at 37 ± 2□ along with 0.1 mg/ml of ascorbic acid to prevent the oxidation of Rif. Sink

176 conditions were maintained by adding 1% tween in PBS which allows the total quantity of drug

177 to be eluted from nanocarrier and reduced adhesion by using dialyzing membrane. The sample

178 was set at 50 rpm and at specific time intervals (1, 2, 4, 8, 12, 24, 48, 72 h), the samples were

179 withdrawn and replaced with fresh medium of the same volume and drug content determined

180 through HPLC method described in section electronic supplementary information [18].

181 ## 2.3 Detection of buffering potential of the polymeric carriers

182 Acid base titration was used in order to evaluate the buffering potential of Chitosan (Ch),

183 Thiolated chitosan (TCh), S-protected thiolated chitosan (PTCh) and Mannosylated S-protected

184 thiolated chitosan (MPTCh). Briefly, the polymeric NCs were dissolved in 0.1N NaCl at a

185 concentration of 0.1mg/ml with pH adjustment of 10. Afterwards, 0.1 M HCl was added

186 dropwise (20 µl) into the polymer solution while different pH values were measured by using pH

187 meter. The slope of the plot between pH and HCl amount indicated the buffering capacity of our

188 polymeric system [4]**.**

189 ## 2.4. Biocompatability, macrophage uptake, mycobacterial inhibition potential and P-gp
190 ## inhibition studies

191 ### *2.4.1 Bacterial culture*

192 *Mycobacterium* strains (H37R_V and R-1343) were obtained from National Reference Laboratory,

193 National Institute of Health, Islamabad, Pakistan. The strains were grown in the mycobacterium

194 growth indicator tube (MGIT 960) added with OADC (oleic acid, albumin, dextrose and

195 catalase) along with antibiotic combination (PANTA) to inhibit the growth of any other bacterial

196 strain and to prevent contamination

197 *2.4.2 Macrophage isolation and infection*

198 Macrophages were isolated from female swiss albino mice using previously reported method
199 [19]. All the animal experiments were approved by the local ethical committee i.e. from
200 bioethical committee Quaid-i-Azam University, Islamabad (BEC-FBS-QAU2019-202) which are
201 approved according to the ARRIVE guidelines and the U.K. Animals (Scientific Procedures)
202 Act, 1986 and associated guidelines. The animals of $20\text{-}25 \pm 5$ g were kept under 12 h light and
203 12 h dark cycles with free access to food and water. Animals were acclimatized for 3-4 weeks
204 and their body weights were measured in order to evaluate the health of the animals and to
205 ensure if they were in an excellent state to perform any experimentation upon them. The animals
206 were used in minimum possible number and the methods applied give minimum stress to
207 animals. Also the sacrifice of animals was done to give the less possible pain of death. Briefly,
208 1.5 ml of sterile thioglycolate (3% w/v) was inoculated into the peritoneal cavity of swiss albino
209 mice. After 3 days the mice were euthanized and ice cold RPMI (5ml) was injected into the
210 peritoneal cavity of mice. The peritoneal exudate was then collected and recovered. The exudate
211 collected above was then processed further followed by the centrifugation of 10 min at 3000
212 rpm. The pellet recovered was then suspended in RPMI supplemented with penicillin,
213 streptomycin and 10% FBS.

214 *2.4.3. Biocompatability analysis and phagocytic uptake*

215 The detailed methodology of biocompatibility and uptake (phagocytic uptake, florescent uptake
216 and uptake *via* flow cytometry) are given in supplementary information.

217 *2.4.4. Treatment with nanoformulations, % inhibition and drug influx by P-gp inhibition*

218 *Macrophage infection*

219 Macrophages isolated above were plated on 24-well plate at the density of 1×10^5 cells/well with
220 microscopic slides and incubated at 37°C in CO_2 incubator for 24h to attach the monolayers to
221 the slides. After incubation, cells were washed with the serum free medium and adherent cells
222 were infected with the *M.tb* at a ratio of 10:1 (*Mycobacteria*: macrophages) and then incubated
223 for 7 days in a CO_2 incubator at 37°C. Afterward, the cells were washed with the RPMI to
224 remove the un-phagocytosed *Mycobacteria* and then incubated with different concentrations of
225 Rif and NC (1-200 µg/ml) for 24 h to examine the bacteria within infected macrophages an acid-

226 fast bacilli (AFB) stain kit (BD Biosciences, country) was used and staining was performed

227 according to the manufacturer's instructions. The slides were then stained with the Giemsa staining

228 solution for 10 min. The stained cells were then visualized under the light microscope to count 100

229 cells per well to compute the percentage of infected macrophages per 100 cells. Percentage of

230 inhibition was calculated by the following equation [20].

$$\% \ inhibition = \frac{No.\ of\ mycobacteria\ in\ control\ well - No.f\ mycobateria\ in\ treated\ well}{No.\ of\ mycobacteria\ in\ control\ well} \times 100$$

231 In order to evaluate the drug uptake of NC by P-gp efflux pump inhibition, the macrophages

232 isolated above (1×10^5 cells/well) and infected with M.tb were treated with adenosine triphosphate

233 binding cassette (ABC) inhibitor i.e. verapamil (5 μM) before adding the NC (at their MICs).

234 Verapamil was added in resistant strain (R1343) infected macrophages, sensitive strain (H37R$_V$)

235 infected macrophages and non-infected macrophages. After treatment of 2 h, cells were washed

236 with buffer (pH 7.4) and treated with Rif and nanocargoes. After 24 h the cells were processed

237 for the HPLC analysis of drug [20].

2.5. Detection of phagosomal maturation and acidification

239 The macrophages cells were isolated from the peritoneal cavity as described above. The

240 macrophages (1×10^5 cells/well) infected with M.tb were exposed to the prepared NCs i.e.

241 MPTCh-NCs (1 µg/ml) for 24 h and then incubated with accredin orange (AO) for 15-20 min in

242 order to detect the acidic vesicular organelles. The acidic compartments fluorescence red color

243 (488 nm) while nucleolus and cytoplasm fluorescence green (520 nm) and this intensity depends

244 on the degree of acidification. The fluorescent microscope (20X) was used to obtain the

245 photomicrographs. To detect the phagosomal acidification upon lysosomal fusion, the treated

246 cells were also stained with Lysotracker-G. After 24 h treatment with nanocargoes, the cells were

247 then washed with PBS and stained with Lysotracker and further incubated at 37^0 C for 15 min.

248 Afterwards the cells were washed with PBS and photomicrographs taken via fluorescent

249 microscope [5, 9].

2.6. Mycothione reductase (MTR) inhibition studies

251 The MTR inhibition studies of S-protected thiomeric NCs on M.tb was conducted as reported

252 previously. Briefly, the crude enzyme (MTR) was prepared by incubating the mycobacterium

253 with lysis buffer (HEPES (40mM), triton-x 100 (2 % v/v), tris (pH 7.5, 50 mM), EDTA (1mM))

254 and phenylmethanesulfonyl fluoride (1mM) was added as protease inhibitor. Total of 75 µl of

255 lysate was added into the 96 well plates along with the addition of 25 µl Ellman's reagent (100

256 µm) and 25 µl NADPH (200 µm) and MPTCh-NCs at different concentrations (0-10 µg/ml). The

257 reaction mixture was then incubated for 3 h in dark at room temperature. After incubation the

258 absorbance was measured at 405 nm using the microwell plate reader [21]. For each sample the

259 control was set by adding all reagents except substrate. To calculate MTR activity following

260 formula was used:

261   MTR = Optical density of sample at 405 nm – Optical density of control at 405 nm

262 Different kinetic models were applied by using Graphpad Prism (model etc) and the R^2 values

263 were subjected to sum of square F-test analysis for best fit values. The IC50 value for MPTCh-

264 NC was calculated by using graph pad prism.

265 **2.7. Detection of oxidative burst, nitric oxide and cytokines quantification**

266 In order to appraise the oxidative burst inside the macrophage cells induced after the uptake of

267 the MPTCh-NC, the macrophages (1×10^5 cells/well) were incubated for 30 min with 2', 7'-

268 dichloroflorescein diacetate (DCFD) which is a cell permeable fluorogenic dye. Afterwards, the

269 cells were then treated with MPTCh-NCs at a concentration of 1 µg/ml. The plate was then kept

270 in dark on a shaker for 10 min and the fluorescence fervency was measured at 485 nm (excitation

271 wavelength) and 530 nm (emission wavelength) by using fluorescent microplate reader [22].

272 The details of the nitric oxide and cytokines quantification are given in supplementary

273 information section.

274 **2.8. Cell annihilation analysis**

275 The cell annihilation after the predisposition of the cells to MPTCh-NCs was evaluated by

276 annexin-V PI staining and then quantitatively assessed by using flow cytometry. Macrophages

277 (1×10^5 cells/well) were seeded in 6 well-plates, infected with M.tb and further incubated for 24

278 h after treatment with pure drug and NCs (Ch, TCh, PTCh and MPTCh) at a concentration of 1

279 µg/ml. Afterwards, the cells washed with PBS and fixed with ice cold methanol (-20^0 C).

280 Subsequently, the fixed cells were embraced with RNase and stained with annexin-V PI and kept

281 in dark for 30 min. Afterwards the fluorescence was measured by flow cytometer for each
282 individual nucleus [5].

283 The nuclear morphological changes provoked by the treatment of NC was enumerated after 4',
284 6'- diamidino-2-phenylindole (DAPI) staining which is a nuclear stain dye. The infected cells
285 were seeded (0.2×10^6 cells/well) in a 6 well-plate and treated with MPTCh-NCs (1 µg/ml) and
286 further incubated for 24 h. Subsequently, the cells were fixed in 4 % paraformaldehyde after
287 washing with PBS. Afterwards, the cells were lysed with lysis buffer (triton X-100) and
288 incubated with DAPI (0.5 µg/ml) for 5 min and visualized under fluorescence microscope [23,
289 24].

290 **2.9. Drug susceptibility testing and *Mycobacterial* EP inhibition**

291 Drug susceptibility testing (DST) and *mycobacterial* efflux pump inhibition potential of the
292 prepared NC was carried out by using growth indicator tubes, MGIT-960 based method (TB
293 Alliance protocol NC-005-(J-M-Pa-Z)) against M.tb and MIC was determined. MGIT growth
294 indicator tube with BACTEC MGIT-960 supplement was used for the *Mycobacterium* in the
295 instrument. The standard protocol was carried out for all the primary drugs. The culture used for
296 inoculation was dispersed to avoid clumps and to allow even distribution of the microbe. After
297 15 min these dispersed cultures were used to inoculate the MGIT tubes containing first-line
298 drugs and ODAC (oleic acid, dextrose, albumin and catalase) supplement. The tubes were then
299 loaded in the MGIT-960 instrument. When GU reaches 400 the instrument reads the set of DST
300 as complete. The complete set was then removed from the instrument and print of the removed
301 DST set was taken an interpreted manually. In comparison to control (GU = 400), if drug-
302 containing tubes showed GU of greater than 100, the result was interpreted as resistant. While, if
303 GU is equal to or less than 100, the result will be interpreted as susceptible. The above
304 experiment was repeated for Rif + Ver and NC (Ch, TCh, PTCh and MPTCh) with different
305 concentrations (0.65-100 µg/ml) in order to estimate the minimum inhibitory concentration
306 (MIC) and EP inhibition potential [7, 25]. The modulation factor (MF) was also calculated by the
307 following formula:

$$MF = \frac{\text{MIC of Rif /NCs}}{\text{MIC of Rif + Verapamil}}$$

2.10. RV1258 inhibition potential by RT-PCR and *in vivo* bioavailability studies

For RV1258 inhibition potential of prepared mannose coated S-protected thiolated NC of Rifampicin, the standard protocol of RT-PCR was used with slight modifications [7].

Mycobacterial cultures (drug sensitive and drug resistant) were obtained from national reference laboratory, NIH Islamabad Pakistan. The strains were incubated at 37^0C with Rif and MPTCh-NCs at their minimum inhibitory concentrations in 7H9 broth containing ODAC (oleic acid, dextrose, albumin and catalase) medium.

RNA extraction from the *Mycobacterial* cultures grown at OD of 600 nm of 0.5 and 0.8 was done by using triazole method. Briefly, the culture was centrifuged at 4000 rpm for 20 min at 25^0C and the pellet was resuspended in 1ml triazole reagent (Invitrogen, USA) in order to lyse the *Mycobacterial* culture and incubated at room temperature for 5 min. Afterwards 400µl of chloroform was added and further incubated for 3 min. The homogenate was then centrifuged at 12000 rpm at 4^0C for 10 min for phase separation. Upper aqueous layer was then separated and isopropanol was added in equal ratio. The tubes were then incubated on ice (-20^0C) for 10 min to precipitate down the RNA. The sample was then centrifuged at 12000 rpm and 4^0C for 10 min and supernatant was discarded. The pellet was dried in the air and afterwards, 40 µl of RNAse free water was added. RNA can be stored at -80^0C until further use. The quality and quantity of RNA was assessed by using Nanodrop plate (Skanit RE 4.1, Thermoscientific). Absorbances were measured at 260, 280 and 320 nm.

RNA isolated above was then reverse transcribed into cDNA by using cDNA synthesis kit (Vivantis cDSK 01-050) and quantitative real time PCR conducted by using 2X HOT SYBR Green qPCR mix (Solar Bio Cat. No. SR1110). The primers used for RV1258 and housekeeping gene are (RV1258c_F: GGCCGCGGGTGATGCCGTCTCGAT, RV1258c_R: ATGCCGCCAACCGTCGCGATCATCAAG, DNAPolA_F: TCGATTGCCGGTTCTTCAC, DNAPolA_R: CACCACGGCTCACACTTTAT). Real time PCR was performed on Mic PCR (Bio Molecular system) and the expression levels were then normalized to the expression level of the reference gene RV1258 [7].

Male BALB/C mice were used for *in vivo* analysis. All the animal experiments were approved by the local ethical committee i.e. from bioethical committee Quaid-i-Azam University, Islamabad

337 (BEC-FBS-QAU2019-202). The details have also been given in the previous section (2.4). The
338 mice (20-25g) were fasted overnight with free access to water and were randomly distributed
339 into four groups (n = 4). Rifampicin loaded NC such as MPTCh and marketed product of
340 Rifampicin at a dose of 12 mg/kg body weight were administered to the mice by oral gavage.
341 Blood samples (approximately 1 ml) were collected from the tail vein at different interval of 1, 4,
342 6, 8, 10, 12, 24, 48 and 72 h in microcentrifuge tubes containing heparin. These blood samples
343 were centrifuged at 3500 r.p.m. for 10 min to separate the plasma, and the plasma samples were
344 then subjected to HPLC analysis [26]. The validated HPLC method was employed as described
345 in supplementary information.

346 **2.11. Statistical analysis**

347 The measurement of the significance of results was carried out by using one-way ANOVA
348 following Tukey's post-hoc test and student t-test where applicable. The $P < 0.05$ was
349 considered as significant. All the results were expressed as the mean ± standard deviation of at
350 least three (n=3) experiments.

351 **3. Results and discussion**
352
353 **3.1. Synthesis, basic characterization and buffering potential of functionalized polymeric
354 nanocargoes**

355 Detailed synthesis and basic characterization of Ch, TCh, PTCh and MPTCh polymers have been
356 presented in supplementary information. The structure of the final product, MPTCh is shown in
357 **Figure 1**. A schematic representation of preparation of MPTCh is give in **Figure S1**. The results
358 of ^{1}H NMR and FTIR analysis are shown in **Figure S2 and Figure S3.** DSC, TGA and XRD
359 **(Figure S4)** are provided in supplementary information section. Briefly, the presence of proton
360 peaks (7-9 ppm) in the 1H NMR spectrum of S-protected thiolated chitosan are associated with
361 aromatic ring of 6-mercapto nicotinic acid (MNA) and presence of methylene peaks (2.7 ppm
362 and 3.5ppm) in spectrum of mannosylated S-protected thiolated chitosan confirmed attachment
363 of sugar moiety to the polymer. The presence of amide, aromatic and hydroxyl bands in FTIR
364 spectra of MPTCh confirms the association of mercaptonicotinc acid and mannose sugar to the
365 polymeric backbone. The DSC analysis of PTCh showed an endothermic peak at 240□ and
366 MPTCh showed an endothermic peak at 260□ with no crystalline melting peak. XRD pattern

367 showed somewhat crystalline nature of all the functionalized polymers. . The crystalline peaks in

368 case of MPTCh-NCs was destroyed which suggests the greatest disarray of the polymer network

369 by the cross linking of polymer with the TPP so the XRD pattern of MPTCh-NCs suggests

370 somewhat amorphous nature of the nanocargoes.

371 Characterization of polymers (in terms of thiol contents, disulfide bonds, amount of S-protected

372 ligand and mannose groups) is given in **Table S1**. Nanoformulations were prepared using the

373 optimized ratios obtained through Design Expert® presented in supplementary material **Table S2**.

374 The third formulation block suggested by Design Expert® was selected for the optimized ratios to

375 prepare the nanoformulations. The results of the hydrodynamic diameter, zeta potential,

376 encapsulation efficiency (EE) and polydispersity index (PDI) for Ch (chitosan), TCh (thiolated

377 chitosan), PTCh (s-protected thiolated chitosan), and MPTCh-NCs (mannosylated s-protected

378 thiolated chitosan) are presented in **Table 1 and Figure 2A (i-iv)**. Based on the impact of

379 particle size, PDI and EE one point at the optimal area was selected at which the particle size

380 was reduced with maximum EE and suitable PDI ($p < 0.5$). Free amino groups at the polymeric

381 surface was involved in cross linking of carrier with TPP and resulted in the spherical shaped

382 NCs [28]**.** Ch-NC exhibited the maximum value (36.3 ± 2) of zeta potential while the MPTCh-

383 NC showed a minimum value (18.4 ± 5.46) of zeta potential. This minimum value of zeta

384 potential is due to the modification of free amino groups of chitosan with thiol and mannose

385 groups. Also, the positive zeta potential of NCs is favorable for their internalization into cells,

386 given that the electrical potential of the cell membrane is negatively charged. S-protected

387 thiomeric chitosan coating provides the steric shielding of NCs from precipitation and

388 aggregation by the proteins in the physiological media. These results indicated the robust

389 stability of nanocarriers which assures the longer circulation time and more chances of

390 macrophage accumulation resulting in enhanced therapeutic efficacy [27].

391 The SEM images of blank MPTCh-NCs and Rif loaded MPTCh-NCs are shown in **Figure 2B,**

392 which indicated a smooth surface of the spherical particles.

393 Drug release from biodegradable polymeric systems follows diffusion (through water filled pores

394 or the matrix following osmotic gradient), erosion (both surface and bulk erosion) and

395 degradation (chemical and enzymatic degradation) [28].

396   One of the dominant cellular uptake mechanisms is endocytosis. This pathway consists of
397   endosomal vesicles which grow in the form of early and late endosomes before fusion with
398   lysosomes and contains degradative enzymes. This results in limited delivery of drugs and
399   macromolecules to intracellular targeted sites. Several attempts have been made to directly
400   deliver the drugs inside the cytosol thus escaping the endocytic pathway [29]. The endosomal
401   escape potential of NCs depends on the inbred buffering capacity of the polymeric carrier The
402   quantity of the HCl imperative to bring the pH decrement from 10 to 2.6 increased in the order
403   NaCl > TCh > Ch > PTCh > MPTCh confirming the accentuated buffering potential of MPTCh
404   because of –NH2 groups of preactivation. **(Figure 3A)**. The results of pure drug suspension
405   showed maximum release (> 80%) in the first 4 h. Rif release from NCs **(Figure 3 B, C)**
406   followed a biphasic release pattern with initial burst release of drug close to particle surface or
407   near the water layer followed by sustained release due to slow diffusion. In general, compared to
408   a pure drug suspension, NCs showed pH-dependent release with initial burst release (˜ 30%)
409   within first 10 h followed by a sustained release for up to 72 h. Notably, TCh-NCs and PTCh-
410   NCs showed better control than pure drug (Rif) and Ch-NCs, releasing 80% drug after 72 h.
411   Generally, chitosan shows a pH-dependent drug release i.e. better drug release at lower pH (pH
412   1-2). This might be attributed to the presence of a more complex and stronger matrix system in
413   the order TCh > PTCh > MPTCh, providing better control over drug release. Rif release kinetics
414   from NC was evaluated by employing various release models for both pH 7.4 and 5.5 release
415   profiles and the results are presented in **Table 2.** Based on the value of R^2, the drug release from
416   Ch-NCs followed first order release behavior at both pH 5.5 and 7.4 and the Rif release from
417   TCh-NCs, PTCh-NCs and MPTCh-NCs followed the Korsmeyer-Peppas model. At pH 7.4 the
418   release followed non-Fickian mechanism as the value of *0.45 < n< 0.89*, that supported
419   relatively larger drug release as shown in **Figure 3B**. The diffusional exponent (n) of
420   Korsmeyer-Peppas model showed the release profile of TCh-NCs, PTCh-NCs and MPTC-NCs
421   followed Fickian at pH 5.5 due to the value of *n < 0.45*, which is evident in **Figure 3C** showing
422   less drug release.

423   **3.2 Biocompatibility, uptake, *Mycobacterial* inhibition and P-gp inhibition analysis**

424   Biocompatibility assessment is an important parameter to study the response of living systems
425   towards NC following administration in time and dose-dependent manners. Though chitosan and

426 its derivatives have been shown as less toxic and more biocompatible, yet NCs may induce some

427 acute or moderate levels of toxicity based on their extremely small size. These toxic effects could

428 be minimized or avoided by surface modification or tuning their properties [30]. The

429 antimycobacterial activity of NC was investigated against M.tb in a concentration-dependent

430 manner. Free Rif was used as a control. As shown in **Figure 4A.** The Rif, Ch, TCh, PTCh and

431 MPTCh-NCs showed $40.9 \pm 2\%$, $60.34 \pm 1\%$, $71.98 \pm 6\%$, $80 \pm 5\%$ and $88.09 \pm 4\%$ growth

432 inhibition respectively. The measured IC_{50} of Rif, Ch, TCh, PTCh, and MPTCh-NCs was found

433 to be 8.71 ± 0.4, 5.82 ± 0.5, 4.55 ± 0.3, 4.04 ± 0.1 and 3.18 ± 0.5 µg/ml respectively (**Figure**

434 **4B**).

435 The biocompatibility of as-prepared NC was evaluated on fresh albino mice peritoneal

436 macrophages using MTT assay. The macrophages were incubated with various concentrations of

437 NCs i.e. 1-200 µg/ml. The results (**Figure 4C**) showed significant ($p < 0.05$) differences among

438 various treatment groups. The results of MPTCh-NCs showed $> 89 \% \pm 2$ cell survival over 24 h

439 at the highest concentration tested (200 µg/ml), while Ch-NCs, TCh-NCs, and PTCh-NCs

440 showed cell survival of 67 ± 7, $81 \pm 10\%$ and $83 \pm 5\%$ respectively at the concentration of 1-200

441 µg/ml. Similarly, MPTCh-NCs and PTCh-NCs showed e significantly ($p < 0.05$) low IC_{50} of 3.6

442 µg/ml and 4.04 µg/ml against macrophages as compared to TCh-NCs and Ch-NCs indicating a

443 lower toxicity of the developed MPTCh-NCs. The values for negative control (Triton X-100, 2%

444 v/v) and positive control (RPMI media) showed $5 \pm 1\%$ and $99 \pm 2\%$ viability respectively.

445 Improved biocompatibility of PTCh-NCs and MPTCh-NCs as compared to the chitosan is

446 attributed to the positive charge density of the chitosan that might have interacted with

447 negatively charged cell membrane.

448 Macrophage surfaces harbor mannose receptors that are over expressed in infected macrophages.

449 PTCh and MPTCh showed increased uptake in both uninfected and H37Rv infected

450 macrophages compared to Rif. This enhanced trafficking inside the macrophages may be

451 attributed due to mannose receptors endocytosis as well as S-S/S-H exchange reaction of S-

452 protected thiomer with the cell membrane [31]. Different studies provide the evidence of

453 effectiveness of thiol moieties present on NC surface in increased internalization. The cell

454 surface thiols further enhance the intracellular uptake of disulfide conjugated thiomeric polymer

455 (PTCh).

456   The fluorescent microscope images of FITC-MPTCh-NCs and macrophages with successful

457   internalization of FITC-MPTCh-NCs are shown in **Figure S 5 (A-B)**. The green fluorescence

458   exhibited by macrophages confirmed the presence of FITC-MPTCh-NCs inside the

459   macrophages. The increased fluorescence inside macrophages was because of the successful

460   disulfide mediated endocytosis as well as mannose receptor-ligand conjugation which showed

461   successful internalization of NCs as a whole, showing the stability of formulation until it reaches

462   the intracellular microenvironment.

463   One of the resistance mechanism associated with TB drugs is the presence of efflux transporters

464   present on macrophages as well as M.tb surface [3].The macrophage uptake of Rif, Ch, TCh,

465   PTCh, and MPTCh-NCs were evaluated both in infected (sensitive and resistant strains)

466   macrophages and uninfected macrophages in the presence of verapamil to evaluate the P-gp

467   inhibition potential. The results presented in **Table 3** showed that Rif exhibited significantly

468   reduced uptake ($P < 0.05$) in macrophages infected with resistant strains. In the case of Ch-NCs

469   and PTCh-NCs the sensitive strain infected macrophages exhibited an uptake of 10.87 ± 0.25 µg

470   Rif/10^6 cells and 34.89 ± 0.24 µg Rif/10^6 cells respectively. It is worth noticing that in case of the

471   resistant strain infected macrophages, PTCh-NCs and MPTCh-NCs exhibited an uptake of 35.24

472   ± 0.01µg Rif/10^6 cells and 76.61 ± 0.05 that is almost equal ($P > 0.05$) to that of sensitive strain

473   infected macrophages i.e. 34.89 ± 0.24 µg Rif/10^6 cells and 76.88 ± 0.02 µg Rif/10^6 cells,

474   respectively. . These results indicated that thiolated NC have successfully inhibited the P-gp EP

475   by developing a disulfide linkage with their cystine subunit [32]**.** MPTCh-NCs exhibited

476   maximum intracellular accumulation of Rif in all cases (non-infected, sensitive strain infected

477   and resistant strain infected macrophages) compared to that of other NCs due to the macrophage-

478   targeted potential of MPTCh-NCs. Hence, these NC might prove to be a suitable strategy to

479   enhance the intracellular accumulation by blocking these EPs [33].

480   **3.3 Phagosomal lysosmal maturation and acidification**

481   M.tb has emerged as an innovative strategy to circumvent the phagolysosomal degradation *via*

482   knockdown of phagosomal maturation processes. We hypothesize that the uptake of MPTCh-

483   NCs could potentially enhance the lysosome accumulation resulting in an increased phagosomal

484   maturation within infected macrophages. The accrual of green fluorescence fervency after

485   MPTCh-NCs treatment indicated the phagosomal maturation and lysosomal buildup as depicted

17

486   in **Figure S 5 (C-D)**. Carrier system developed in the present work releases the phagosomal

487   maturation block and enhances the *Mycobacterial* insult. Based on these results, it can be

488   concluded that MPTCh-NCs could play a vitol role in autophagy within *Mycobacterium* infected

489   macrophages, although the mechanism has not been illustrated yet. Future studies should

490   emphasize on the exploring this mechanism.

491   **3.4 Mycothione reductase (MTR) inhibition assay**

492   The maintenance of redox balance is crucial for the survival of M.tb inside the host. To

493   neutralize the oxidative stress of host immune response system, M.tb utilizes the unique

494   protecting enzyme mycothione-reductase (MTR). This NADPH dependent MTR protein ensures

495   the reductive environment by maintaining the mycothiol (MSH) in its reduced form. The

496   inhibition of MTR by thiomers can increase the efficacy of anti-tubercular drugs. The MTR

497   inhibitory activity of MPTCh-NP was evaluated at different concentrations (1-100 μg/ml) against

498   1 μm concentration of Mycothiol (MSH) produced by Mycothione reductase (MTR). The result

499   showed that thiomeric NPs inhibited MTR by competitive mix model **(Figure 5A, 5B)** of

500   inhibition and has Ki value of 2.874 and R^2 value of 0.9988. The enzyme inhibition activity was

501   plotted against the log concentration of thiomer as shown in **Figure 5C**. The IC_{50} of 4.96 was

502   observed for MPTCh-NP.

503   **3.5 Nitric oxide generation and cytokine evaluation**

504   Griess assay was performed to measure the nitrite levels after treatment with nanoformulations.

505   Nitrite production was found to be in the order MPTCh-NC > PTCh-NC > TCh-NC > Ch-NC

506   when compared to the control group. MPTCh-NC, PTCh-NC, TCh-NC and Ch-NC treated

507   supernatants of macrophages showed higher levels of nitrite i.e. 80.38 ± 9.89μM, 62.72 ±

508   7.98μM, 56.15 ± 5.89μM and 50.95 ± 4.79μM respectively **(Figure 6A)**. While Rif and control

509   groups showed 37.93μM and 25.49μM respectively. Coated formulations showed 4.5 and 2.4-

510   fold increase in nitrite production respectively while uncoated formulations showed 1.51-fold

511   higher amount of nitrite when compared to the control group. The increase in nitrite production

512   by MPTCh-NCs treated cells is due to the up regulation of TNF-α which is involved in restricting

513   the mycobacterium inside macrophages [33]. The increased production of TNF-α and IL-12 by

514   coated NCs was in the order MPTCh-NC > PTCh-NC > TCh-NC > Ch-NC when compared to

18

515 uncoated Rif and the control group. This clearly demonstrates that coated MPTCh-NC

516 potentiates the spontaneous immunological response by activation of macrophages.

517 The immunomodulatory activity of the coated nanoformulations was evaluated in terms of TNF-

518 α, IL-10, IL-12 and IL-6 as shown in **Figure 6 (B-E)** respectively. The coated formulations

519 MPTCh-NC, PTCh-NC, TCh-NC and Ch-NC indicated the TNF-α concentration as 640.84 $\pm$

520 13.45 pg/ml, 510 $\pm$ 10.15 pg/ml, 405.76 $\pm$ 8.73 pg/ml and 350.89 $\pm$ 7.54 pg/ml respectively and

521 IL-12 concentration of 630.66 $\pm$ 13.63, 565.61 $\pm$ 15.40, 525.49 $\pm$ 10.83 and 390.34 $\pm$ 9.59

522 respectively. The TNF-α levels are significantly higher ($p < 0.05$) as compared to uncoated

523 nanoformulations and control. While IL-6 and IL-10 levels indicated no significant difference

524 ($p < 0.05$) between coated (i.e. MPTCh-NC, PTCh-NC, TCh-NC, Ch-NC), uncoated and control

525 formulations. Stability studies of NC in PBS and FBS was determined at 37^{0}C. No substantial

526 change in nanocarrier size was observed in both PBS and FBS up to 1 week at 37^{0}C as shown in

527 **Figure 6F.**

528

529 **3.6 Oxidative spurt and cellular annihilation**

530 Oxidative burst was measured to evaluate the intracellular trafficking of NC towards

531 macrophages after 5 min exposure. ROS was assessed in terms of relative fluorescence units

532 after DCFD staining. According to the data presented in the **Figure 6G**, the relative fluorescence

533 fervency of PTCh treated cells was much higher than that of control, Ch and TCh after 24 h. It is

534 likely that the oxidative burst may occur at the initial stages of interaction of cells with

535 Mycobacterium. Moreover, the oxidative burst in both the untreated control and M.tb control

536 was very low with no significant differences. ROS is generated as a byproduct of oxygen

537 metabolism. Increased ROS production leads to enhanced bacterial killing *via* variety of

538 mechanisms such as oxidative defragmentation or affliction of RNA, DNA and bacterial

539 proteins, augmentation of membrane permeability and lipid peroxidation [34]. These

540 mechanisms lead to bacterial death by augmentation of bacterial oxidative phosphorylation [34,

541 35]. Our findings demonstrated that MPTCh-NCs augmented the generation of ROS.

542 Different studies are concordant with the fact that there is an involvement of different

543 biochemical, physiological and morphological factors associated with apoptosis in prokaryotes

19

544 [5, 9]. Cell death initiated after exposure of infected cells with Rif, Ch, TCh, PTCh and MPTCh-

545 NC was detected by annexin-V and PI staining. The increase in the granularity in PTCh and

546 MPTCh-NCs *via* flow cytometry as shown in **Figure 7 (1) A-G** depicted the increased uptake of

547 MPTCh-NC and PTCh-NC inside the BCG infected macrophages compared to TCh-NC. The

548 cell annihilation was shown in the **Figure 7(2) A-E**. Percentage of early and late apoptotic cell

549 death by flow cytometry analysis is given in **Table S3.** The data suggested the increase in %

550 apoptosis cell treated with different NC compared to control. The increase in apoptosis may be

551 related to DNA stand fragmentation of *Mycobacterium* infected cells by PTCh and MPTCh. The

552 histograms for the apoptosis data are given in supplementary data **Figure S6.** The percentage of

553 apoptotic cells increased to 40.4% for PTCh and 33.29% for MPTCh compared to pure drug Rif

554 i.e. 23.25%. This apoptosis is potentially related to the increased ROS production as well as

555 inhibition of MTR.

556 The resultant fluorescent images demonstrated aberrant margins and dense chromatin with

557 nuclear disintegration shown in supplementary information **Figure S7.** The treatment of 1µg/ml

558 dose of MPTCh exhibited blue clusters indicating nuclear disintegration after staining with

559 DAPI. These results of DNA disintegration and nuclear protuberances further strengthen the

560 concept of cell demise upon MPTCh exposure.

561 **3.7 Drug susceptibility testing and Mycobacterial efflux pump inhibition**

562 The MIC of the Rif, Rif + ver and synthesized NC i.e. Ch, TCh, PTCh and MPTCh-NCs were

563 found to be 2 µg/ml, 0.25 μg/ml, 0.5 μg/ml, 0.25 μg/ml, 0.0625µg/ml and 0.0625 µg/ml

564 respectively for sensitive strain (**Table 4**). The modulation factor (MF) of 8 and 5.33 showed the

565 synergistic microbicidal potential of verapamil by inhibiting the efflux machinery on bacterial

566 surface. Similarly, MIC of the formulation MPTCh-NCs for resistant strain (R-1343) was found

567 to be 16 μg/ml compared to pure drug (256 μg/ml). The increased MF of PTCh-NCs and

568 MPTCh-NCs with a value of 16 showed the synergistic potential of our NC in *Mycobacterial*

569 killing. These results confirmed the significantly superior anti-tuberculosis activity by EP

570 inhibition potential of the synthesized nanocargoes.

571 We also examined the effect of our carrier system at molecular level on gene RV1258 via real

572 time PCR in order to quantify the gene expression level after MPTCh-NC treatment. The results

573 are presented in **Figure 8A**. There was a substantial 8.13 folds lower expression on RV1258

574 level after MPTCh-NC treatment in comparison to pure drug Rif. The significant decrease in

575 gene expression level in comparison to controls and Rif suggests the strong possible evidence of

576 involvement of our carrier system in *Mycobacterial* efflux pump inhibition. The decreased MIC

577 values, enhanced modulation factor and decreased expression of RV1258 of as-prepared S-

578 protecetd thiomeric carrier system against resistant strain is potentially due to the inhibition of

579 the efflux pump (RV1258) which is involved in the expulsion of Rif [7].

580 **3.8 *In vivo* bioavailability and stability analysis**

581 Reduced antimycobacterial drug concentrations such as Rif and INH and reduced functional

582 absorptive area of intestine in TB patients are major concerns limiting the selective and targeted

583 efficacy of drugs. Therefore, it is significantly important to develop new drug delivery

584 approaches in order to improve the bioavailability of these drugs. In order to evaluate the oral

585 bioavailability of prepared MPTCh-NCs, the BALBc mice were orally administered the

586 marketed Rif and Rif-loaded MPTCh-NCs. Mean plasma drug concentrations against different

587 time intervals are shown in the **Figure 8B.** The depicted value of AUC of MPTCh-NCs was

588 12.31 folds higher in comparison to marketed Rif product. As-prepared MPTCh-NCs

589 demonstrated effectively increased bioavailability compared to conventionally used products

590 which make this NC-based platform an ideal therapeutic agent to treat TB while remaining non-

591 toxic to surrounding tissues/cells.

592 **4. Conclusion**

593 This work demonstrated the novel development of S-protected thiomeric site-specific

594 nanocargoes (NCs) of Rifampicin (Rif) for the controlled and sustained release of Rif to target

595 the ROS-mediated cell death. NCs also exhibited sustained and slow release of drug, revealing

596 the enhanced endosomal escape potential as well as phagolysosomal fusion. Rapid efflux of drug

597 was demonstrated by the over expression of bacterial efflux proteins (EPs) such as RV1258.

598 Moreover, *in vitro* studies demonstrated the potential of biocompatible NCs in enhancing

599 intracellular drug uptake by suppression of macrophage and bacterial efflux machinery as

600 evident from the increased MF. As-prepared NCs also exhibited improved bioavailability *in vivo*.

601 These findings provide a proof-of-concept that as-prepared NCs were efficient in eradicating

602 intracellular pathogens and can be further explored for their immune regulation potential. Taken

603 together, our findings based on *in vitro* and *in vivo* experiments could be used in solving real-
604 world clinical problems related to TB.

605 **4. Author statement**

606 **Aisha Rauf:** Conceptualization, investigation, methodology, software, writing and editing;
607 **Sobia Razzaq:** Software, analysis; **Tanveer A Tabish:** Reviewing and editing; **Sabira**
608 **Tahseen:** Supervision, Resources, Validation; **Mansoor Abdullah Sandhu:** Resources,
609 validation, investigation, formal analysis; **Gul Shahnaz:** Supervision, methodology, writing-
610 reviewing and editing.

611 **5. Declaration of competing interest**

612 The authors declare no conflict of interest.

613

614

615

616

617

618

619

620

621

622

623

624

625

626

Table 1: Characterization of various nanoformulations in terms of mean particle size, polydispersity index (PDI), encapsulation efficiency (EE) and zeta potential

Formulation	Diameter (nm)	EE (%)	Zeta potential (mV)	PDI
Ch-NPs	276 ± 17	73.3 ± 19.2	36.3 ± 2	0.369 ± 0.001
TCh-NPs	288 ± 13	78.8 ± 12.1	26.2 ± 8.19	0.381 ± 0.4
PTCh-NPs	381 ± 15	87.6 ± 18.6	24.5 ± 5.13	0.325 ± 0.09
MPTCh-NPs	390 ± 20	73.68 ± 5.99	18.4 ± 5.46	0.385 ± 0.05

Ch-NPs= Chitosan Rif nanoparticles, TCh-NPs= thiolated chitosan Rif nanoparticles, PTCh-NPs= pre-activated thiolated chitosan Rif nanoparticles, MPTCh-NPs= mannosylated pre-activated thiolated chitosan Rif nanoparticles.

Table 2: Drug release data modeling based on *in vitro* Rifampicin release from various nanoformulations to determine possible drug release mechanisms

Formulation code	Zero-order $C_t=C_0+k_0t$		First order $\log Q_0+K_it/2.3$		Higuchi model $f_1=Q=K_H\sqrt{t}$		Korsmeyer-Peppas model $M_i/M_\infty=Kt^h+b$		Hixson-Crowell model $3\sqrt{W_i}+K_{HC}t$	
	K0	R^2	K0	R^2	K0	R^2	N	R^2	K0	R^2
pH 7.4										
Ch-NPs	1.92	0.392	0.088	**0.984**	14.10	0.878	0.400	0.902	0.020	0.947
TCh-NPs	1.48	0.533	0.038	0.911	10.69	0.963	0.42	**0.973**	0.011	0.849
PTCh-NPs	1.08	0.296	0.018	0.602	7.445	0.902	0.409	**0.955**	0.011	0.511
MPTCh-NPs	0.69	0.085	0.010	0.123	5.22	0.787	0.413	**0.966**	0.003	0.050
pH 5.5										
Ch-NPs	1.981	0.374	0.097	**0.985**	14.59	0.87	0.428	0.909	0.021	0.931
TCh-NPs	1.68	0.615	0.050	0.970	12.40	0.970	0.467	**0.973**	0.014	0.936
PTCh-NPs	1.48	0.727	0.034	0.964	10.43	0.988	0.457	**0.988**	0.009	0.930
MPTCh-NPs	1.26	0.807	0.023	0.942	8.73	0.990	0.481	**0.994**	0.006	0.916

Ch-NPs= Chitosan Rif nanoparticles, TCh-NPs= thiolated chitosan Rif nanoparticles, PTCh-NPs= pre-activated thiolated chitosan Rif nanoparticles, MPTCh-NPs= mannosylated pre-activated thiolated chitosan Rif nanoparticles.

Table 3: Comparison of uptake of rifampicin for targeted (mannosylated S-protected thiolated chitosan), S-protected thiolated chitosan, thiolated chitosan and unmodified chitosan and Rif in uninfected and infected macrophages

Uptake studies (µg Rif/10^6 cells)				
Formulations	Uninfected macrophages	Sensitive strain (H37R$_V$) infected macrophages	Resistant strain (R-1343) infected macrophages	P-value
RIF	3.82 ± 0.05	3.58 ± 0.08	2.146 ± 0.45	0.4974x 0.0013 y 0.0035z
Ch-NPs	10.56 ± 0.03	10.87 ± 0.25	5.8 ± 0.01	0.1309x 0.0001 y 0.0001z
TCh-NPs	20.67 ± 0.01	20.41 ± 0.21	20.5 ± 0.15	0.1183x 0.1010y 0.99168z
PTCh-NPs	35.45 ± 0.04	34.89 ± 0.24	35.24 ± 0.01	0.0568x 0.2172y 0.5708z
MPTCh-NPs	76.48 ± 0.02	76.88 ± 0.02	76.61 ± 0.05	0.3310x 0.5377y 0.0812z
Pretreatment with verapamil				
RIF	3.85 ± 0.13	3.67 ± 0.17	2.45 ± 0.03	0.119x 0.0001y 0.0001z
Ch-NPs	10.98 ± 0.25	10.68 ± 0.34	7.45 ± 0.45	0.134x 0.000y 0.0001z

Both sensitive (H37R$_V$) and resistant strains (R-1343) of *M.tb* were used to infect the macrophages. The results are expressed as the mean ± SD of three independent experiments. Ch: chitosan, TCh: thiolated chitosan, PTCh: S-protectedthiolated chitosan, MPTCh: mannosylatedS-protectedthiolated chitosan, x: probability value between uninfected macrophages group and sensitive strain infected group, y: probability value between uninfected macrophages group and resistant strain infected group, z: probability value between sensitive strain infected macrophages and resistant strain infected macrophages group.

Table 4: Drug susceptibility testing (MIC=µg/ml) of *M. tuberculosis* isolates determined by the BACTEC MGIT 960 system

Strain	Rif		Rif+ Ver	Ch	TCh	PTCh		MPTCh	
H37Rv	2	0.25	MF= 8	0.5	0.25	0.0625	MF=32	0.0625	MF=32
R-1343	256	48	MF=5.33	32	32	16	MF=16	16	MF=16

References

[1] W. Organistaion, Global Tuberculosis Report 2016.
https://www.researchgate.net/publication/312655793_Global_tuberculosis_report_2016.

[2] F. Chellat, Y. Merhi, & A. Moreau, Therapeutic potential of nanoparticulate systems for macrophage targeting, Biomat. 26(2005) 7260-7275. https://doi.10.1016/j.biomaterials.2005.05.044.

[3] L. H. M. T. Brake, G. J. D. Knegt, J. E. D. Steenwinkel, T. J. P. V. Dam , J. B. Koenderink, & R. E. Aarnoutse, The role of efflux pumps in tuberculosis treatment and their promise as a target in drug development: unraveling the black box, Ann. rev. Pharm. and Tox. 58 (2018) 271-291. https:// doi.org/10.1146/annurev-pharmtox-010617-052438.

[4] H. Lu, Y. Dai, L. Lv, & H. Zhao, Chitosan-graft-polyethylenimine/DNA nanoparticles as novel non-viral gene delivery vectors targeting osteoarthritis, Plos one. 9 (2014). https://doi.org/10.1371/journal.pone.0084703.

[5] T. K. Upadhyay, N. Fatima, A. Sharma, D. Sharma, & R. Sharma, Nano-Rifabutin entrapment within glucan microparticles enhances protection against intracellular M.tb, Artif. cel., nanomed. biotech. 47 (2019) 427-435. https:// doi: 10.1080/21691401.2018.1559180.

[6] C. J. Hamilton, R. M. Finlay, M. J. Stewart, & A. Bonner, Mycothiol disulfide reductase: a continuous assay for slow time-dependent inhibitors, Ana. biochem. 388 (2019), 91-96. https:// doi: 10.1016/j.ab.2009.02.015.

[7] K. R. Caleffi-Ferracioli, R. F. Cardoso, J. V. de Souza, L. S. Murase, P. H. Canezin, R. B. Scodro, . . . F. R. Pavan, Modulatory effects of verapamil in rifampicin activity against M.tb, Future microbiol. 14(2019) 185-194. https:// /doi:10.2217/fmb-2018-0277

[8] A. Kahnert, P. Seiler, M. Stein, S. Bandermann, K. Hahnke, H. Mollenkopff, & S. H. E. Kaufmann, Alternative activation deprives macrophages of a coordinated defense program to Mycobacterium tuberculosis, Europ. J. Immunol. 36 (2006) 631-647. https:// doi: 10.1002/eji.200535496.

[9] J. Jeevanandam, A. Barhoum, Y. S. Chan, A. Durfresne & M. K. Danquah, Review on anoparticles and naostructured materials: history, sources, toxicity and regulation, Beil. J. Nanotech. 9 (2018) 1050-1074. https://doi.org/10.3762/bjnano.9.98.

[10] J. Pi, L. Shen, E. Yang, H. Shen, D. Huang, R. Wang, . . . J. Cai, Macrophage-targeted Isoniazid-selenium nanoparticles promote innate immunity, inducing synergistic antimicrobial and bactericidal destructions of tuberculosis bacilli, Angew.Chem. Int. Edit. 2019. https://doi.org/10.1002/anie.201912122.

[11] G. Shahnaz, C. Kremser, A. Reinisch, A. Vetter, F. Laffleur, D. Rahmat, . . . R. Tessadri, Efficient MRI labeling of endothelial progenitor cells: design of thiolated surface stabilized superparamagnetic iron oxide nanoparticles, *Europ. J. Pharm. Biopharm. 85* (2013) 346-355. https:// doi:10.1016/j.ejpb.2013.02.010.

[12] H. Friedl, & A. Bernkop-Schnürch, S-Protected Thiolated Chitosan for Oral Delivery of Hydrophilic Macromolecules: Evaluation of Permeation Enhancing and Efflux Pump Inhibitory Properties, Mol. Pharm. 9 (2012) 1331-1341. https://doi: 10.1021/mp200598j.

[13] H. S. Sarwar, M. F. Sohail, N. Soljoughian, et al., Design of mannosylated oral amphotericin B nanoformulation : efficacy and safety in visceral leishmaniasis, NBM. 46 (2018) 521-531. https:// doi: 10.1080/21691401.2018.1430699.

[14] M. F. Sohail, S. Z. Hussain H. Saeed, et al., Polymeric Nanocapsules embedded with ultra small silver nanoclusters for synergistic pharmacology and improved orallof docetaxel, Sci Rep. 8 (2018) 1333. https:// doi:10.1038/s41598-018-30749-3.

[15] G. Shahnaz, , B. J. Edagwa, J. McMillan, S. Akhtar, A. Raza, N. A. Qureshi, . . . H. E. Gendelman, Development of mannose-anchored thiolated amphotericin B nanocarriers for treatment of visceral leishmaniasis, Nanomed. 12 (2017) 99-115. https:// doi: 10.2217/nnm-2016-0325.

[16] M. Sajjad, M. I. Khan, S. Naveed, et al., Folate-Functionalized Thiomeric Nanocargoes for Enhanced Docetaxel Cytotoxicity and Improved Oral Bioavailability, AAPS PharmSciTech. 20(2019) 81. https:// doi: 10.1208/s12249-019-1297-z.

[17]H. Katas, Z. Hussain, & S. A. Awang, Bovine serum albumin-loaded chitosan/dextran nanoparticles: preparation and evaluation of ex vivo colloidal stability in serum, J. Nanomat. (2013) 1-9. https://doi.org/10.1155/2013/536291.

[18] J.-H. Kim, Y.-S. Kim, K. Park, S. Lee, H. Y. Nam, K. H. Min, . . . S. Y. Jeong, Antitumor efficacy of cisplatin-loaded glycol chitosan nanoparticles in tumor-bearing mice. J. Cont. Rel. 127 (2008) 41-49. https:// doi: 10.1016/j.jconrel.2007.12.014.

[19] M. J. Dar, F. U. Din, & G. M. Khan, Sodium stibogluconate loaded nano-deformable liposomes for topical treatment of leishmaniasis: macrophage as a target cell, Drug deli. 25(2018) 1595-1606. https://doi: 10.1080/10717544.2018.1494222.

[20] H. S. Sarwar, S. Ashraf, S. Akhtar, M. F. Sohail, S. Z. Hussain, M. Rafay, . . . G. Shahnaz, Mannosylated thiolated polyethylenimine nanoparticles for the enhanced efficacy of antimonial drug against Leishmaniasis, Nanomed. 13 (2018) 25-41. https:// doi: 10.2217/nnm-2017-0255.

[21] C. J. Hamilton, R. M. Finlay, M. J. Stewart, & A. Bonner, Mycothiol disulfide reductase: a continuous assay for slow time-dependent inhibitors, Ana. biochem. 388 (2019), 91-96. https:// doi: 10.1016/j.ab.2009.02.015.

[22] E. Barcińska, J. Wierzbicka, A. Zauszkiewicz-Pawlak, D. Jacewicz,, A. Dabrowska, & I. Inkielewicz-Stepniak, Role of oxidative and nitro-oxidative damage in silver nanoparticles cytotoxic effect against human pancreatic ductal adenocarcinoma cells, Oxid. med. and cel. long.2018. https://doi.org/10.1155/2018/8251961.

[23] M. S. Ahmed, S. Siddiqui, A. Jaffri, et al., Induction of apoptosis and anti-proliferative activity of naringenin in human epidermal carcinoma cell through ROS generation and cell cycle arrest, Plos one. 9(2014) 102-108. https://doi.org/10.1371/journal.pone.0110003.

[24] U. Lewandowska, K. Sczewczyk, et al., Flavanols from evening primrose (Oenthera paradoxa) defatted seeds inhibit prostate cells invasiveness and cause changes in Bcl-2/Bax mRNA ratio. J. Agri. Food Chem. 61(2013) 2987-2998. https:// doi: 10.1021/jf304269x.

[25] B. Saifullah, P. Arulselvan, M. E. El Zowalaty, S. Fakurazi, T. J. Webster, B. M. Geilich, & M. Z. Hussein, (2014). Development of a biocompatible nanodelivery system for tuberculosis drugs based on isoniazid-Mg/Al layered double hydroxide, Int. J. nanomed. 9 (2014) 4749. https:// doi: 10.2147/IJN.S63608.

[26] R. Pandey, A. Zahoor, S. Sharma, & G. Khuller, Nanoparticle encapsulated antitubercular drugs as a potential oral drug delivery system against murine tuberculosis, Tuber. 83 (2003) 373-378. https:// doi: 10.1016/j.tube.2003.07.001.

[27] G. Shahnaz, C. Kremser, A. Reinisch, A. Vetter, F. Laffleur, D. Rahmat, . . . R. Tessadri, Efficient MRI labeling of endothelial progenitor cells: design of thiolated surface stabilized superparamagnetic iron oxide nanoparticles, *Europ. J. Pharm. Biopharm. 85* (2013) 346-355. https:// doi:10.1016/j.ejpb.2013.02.010.

[28] Y. Fu, &W. J. Kao, Drug release kinetics and transport mechanisms of non-degradable and degradable polymeric delivery systems, Exp. opi. drug deli. 7 (2010) 429-444. https:// doi: 10.1517/17425241003602259.

[29] A. K. Varkouhi, M. Scholte, G. Storm, & H. J. Haisma, Endosomal escape pathways for delivery of biologicals, J. Control. Rel. 15*1* (2011) 220-228. https:// doi: 10.1016/j.jconrel.2010.11.004.

[30] M. F. Sohail, H. S. Sarwar, I. Javed, A. Nadhman, S. Z. Hussain, H. Saeed, . . . G. Shahnaz, Cell to rodent: toxicological profiling of folate grafted thiomer enveloped nanoliposomes, Toxi. res. 6 (2017) 814-821. https;// doi: 10.1039/c7tx00146k.

[31] S. Aubry , F. Burlina, E. Dupont, , D. Delaroche, A. Joliot, S. Lavielle , . . . S. Sagan, Cell-surface thiols affect cell entry of disulfide-conjugated peptides, The FASEB J. *23*(2009) 2956-2967.https://doi.org/10.1096/fj.08-127563.

[32] F. Föger, T. Schmitz, & A. Bernkop-Schnürch, In vivo evaluation of an oral delivery system for P-gp substrates based on thiolated chitosan, Biomat. 27(2006) 4250-4255. https://doi: 10.1016/j.biomaterials.2006.03.033.

747 **[33]** I.Afzal, H. S. Sarwar, M. F. Sohail, S. Varikuti, S. Jahan, S. Akhtar, G. Shahnaz, Mannosylated
748 thiolated paromomycin-loaded PLGA nanoparticles for the oral therapy of visceral leishmaniasis,
749 Nanomed. 14(2019) 387-406. https:// doi: 10.2217/nnm-2018-0038. Epub 2019 Jan 28.
750
751 **[34]** J. Chan, Y. Xing, R. S. Magliozzo, & B. R. Bloom, Killing of virulent M.tb by reactive nitrogen
752 intermediates produced by activated murine macrophages, The J. exp. med. 175(1992) 1111-1122.
753 https:// doi.10.1084/jem.175.4.1111.

754 **[35]** C.-S. Yang, D.-M. Shin, K.-H. Kim, Z.-W. Lee, C.-H. Lee, S. G. Park, . . . E.-K. Jo, NADPH oxidase 2
755 interaction with TLR2 is required for efficient innate immune responses to mycobacteria via cathelicidin
756 expression, The J. immunol. 182 (2009) 3696-3705. https:// doi: 10.4049/jimmunol.0802217.

Manuscript figures captions

Figure1: A schematic representation of final structures of mannose coated S-protrcted thiolated chitosan (MPTCh).

Figure 2: (A) Response surface methodology (RSM) plots of the prepared nanocargoes from MPTCh showing the effect of independent factors on **(a)** size, **(b)** zeta potential, **(c)** encapsulation efficiency (EE) and **(d)** polydispersity index (PDI). **(B)** Scanning electron microscopy (SEM) analysis of the prepared Ch-NCs, TCh-NCs, PTCh-NCs and rifampicin loaded MPTCh-NCs, at 24,000 X magnification.

Rif=Rifampicin, Ch-NCs=chitosan nanocargoes, TCh-NCs=thiolated chitosan nanocargoes, PTCh-NCs=S-protected thiolated nanocargoes, MPTCh-NCs=mannosylated S-protected thiolated nanocargoes.

Figure 3: (A) Proton sponge effect result of Ch, TCh, PTCh and MPTCh polymeric carrier. **(B, C)** Drug release profile of Rif=Rifampicin, Ch-NCs=chitosan, TCh-NCs=thiolated chitosan, PTCh-NCs=S-protected thiolated chitosan, MPTCh-NCs=mannosylated S-protected thiolated chitosan at (B) Ph=7.4 and (C) pH=5.5. values are mean ± SD of three experiments.

Rif=Rifampicin, Ch-NCs=chitosan nanocargoes, TCh-NCs=thiolated chitosan nanocargoes, PTCh-NCs=S-protected thiolated nanocargoes, MPTCh-NCs=mannosylated S-protected thiolated nanocargoes.

Figure 4: Characterization, evaluation and antimycobacterial potential of nanocargoes **(A)** percentage inhibition of M.tuberculosis at different concentrations of nanocargoes (1-200 µg/ml) **(B)** IC_{50} values of nanocargoes against intracellular macrophages **(C)** Biocompatibility of Rif and nanocargoes against laboratory isolated mouse peritoneal macrophages after 24 h incubation. All the results are expressed as mean ± SD of the triplicated experiment, and statistically significant differences were evaluated by one-way ANOVA followed by Dunnett's multiple comparisons test at significance level of **$p < 0.05$.

Rif=Rifampicin, Ch-NCs=chitosan nanocargoes, TCh-NCs=thiolated chitosan nanocargoes, PTCh-NCs=S-protected thiolated nanocargoes, MPTCh-NCs=mannosylated S-protected thiolated nanocargoes, AO= accredin orange.

Figure 5: Mycothione reductase (MTR) inhibition kinetics. **(A)** Lineweaver-Burk plot of MPTCh, **(B)** Non linear fitting of mixed model inhibition of MPTCh and **(C)** Inhibitory activity of Mycothione reductase at different log concentrations of polymer MPTCh and its IC_{50} value.

Figure 6: (A) Production of nitric oxide by the *Mycobacterium tuberculosis* infected macrophages after 72h incubation Rif and nanocarriers of Ch-NC, TCh-NC, PTCh-NC and MPTCh-NC, the data. **(B, C, D, E)** Cytokines evaluation from *Mycobacterium tuberculosis* infected macrophages treated with Rif, Ch-NC, TCh-NC, PTCh-NC and MPTCh-NC by ELISA after 72h incubation. All results are presented as mean ± S.D of experiments performed in triplicate and one-way ANOVA was applied to calculate level of significance**. (F)** Stability studies of MPTCh-NC in PBS and FBS showing robust stability (Mean ± S.D, n=3) **(G)** Fluorescent activity via Reactive oxygen species production. (Mean ± S.D, n=3)

ANOVA= Analysis of variance, PBS= Phosphate buffer saline, FBS= Fetal bovine serum, Rif=Rifampicin, Ch-NCs=chitosan nanocargoes, TCh-NCs=thiolated chitosan nanocargoes, PTCh-NCs=S-protected thiolated nanocargoes, MPTCh-NCs=mannosylated S-protected thiolated nanocargoes.

Figure 7: (1) Uptake of Nanocargoes by flow cytometry **(A)** Non- fluorescent mycobacterium (H37Rv) **(B)** Florescent dsRed BCG strain **(C)** Uptake of Rifampicin treated dsRed BCG strain **(D)** Uptake of Ch-NCs treated dsRed BCG strain **(E)** Uptake of TCh-NCs treated dsRed BCG strain **(F)** Uptake of PTCh-NCs treated dsRed BCG strain **(G)** Uptake of MPTCh-NCs treated dsRed BCG strain. **(2)** Apoptosis study via flow cytometry showing the apoptosis potential of **(A)** Rif **(B)** Ch-NCs **(C)** TCh-NCs **(D)** PTCh-NCs **(E)** MPTCh-NCs

Rif=Rifampicin, Ch-NCs=chitosan nanocargoes, TCh-NCs=thiolated chitosan nanocargoes, PTCh-NCs=S-protected thiolated nanocargoes, MPTCh-NCs=mannosylated S-protected thiolated nanocargoes.

Figure 8: (A) Gene expression level of RV1258 by real time PCR. All results are presented as mean ± S.D of experiments performed in triplicate and one-way ANOVA was applied to calculate level of significance.(Mean ± S.D, n=3) **(B)** Plasma concentration V/S time curve plot of commercial Rif and MPTCh-NCs. All results are presented as mean ± S.D of experiments performed in triplicate (Mean ± S.D, n=3)

MPTCh-NCs=mannosylated S-protected thiolated nanocargoes, D271= Rif resistant mycobacterial strain, H37Rv= wild type mycobacterial strain, Rif= Rifampicin
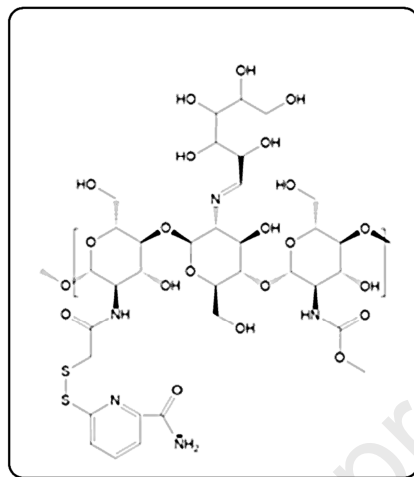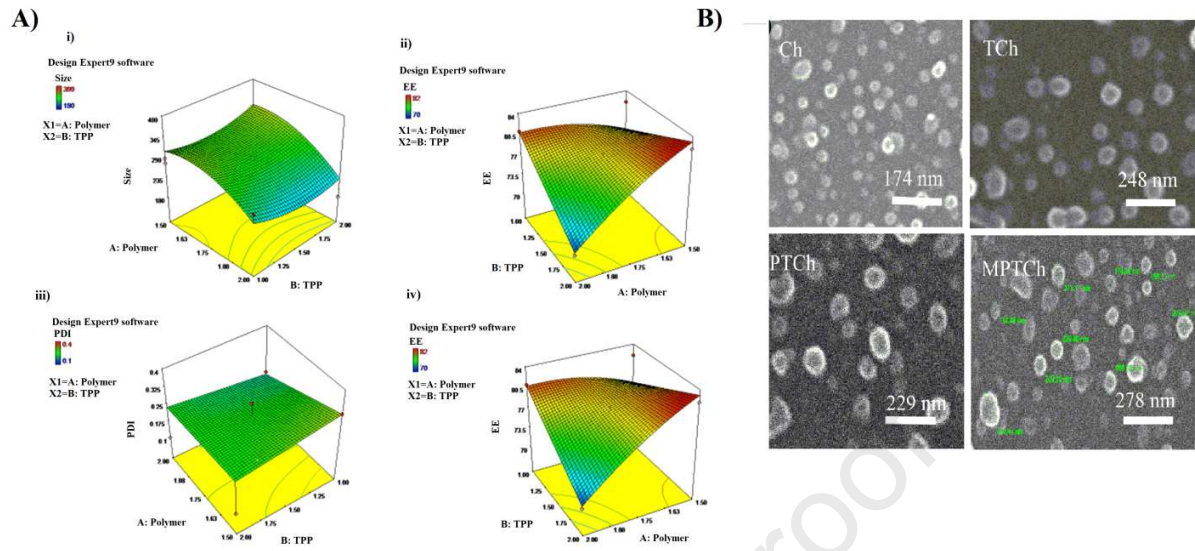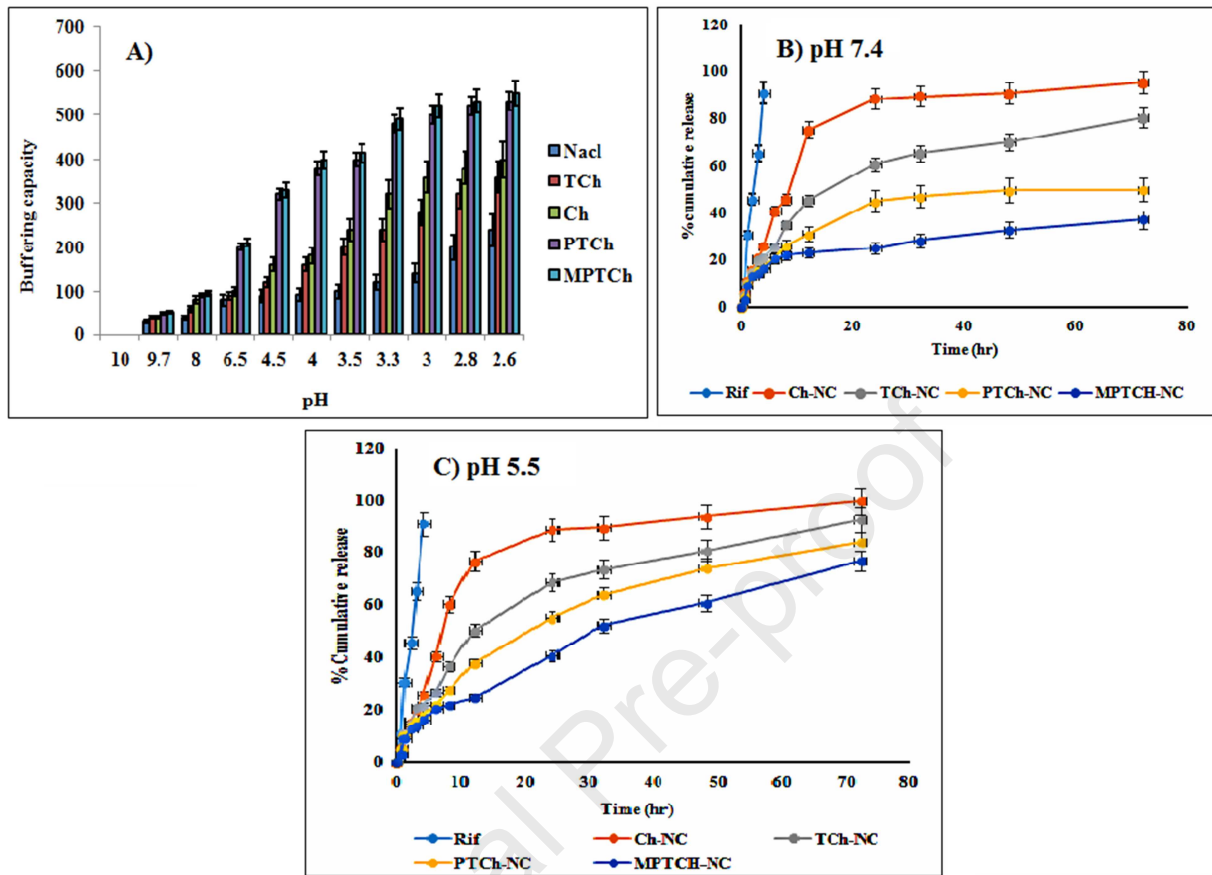
Figure 1

Figure 2

Figure 3
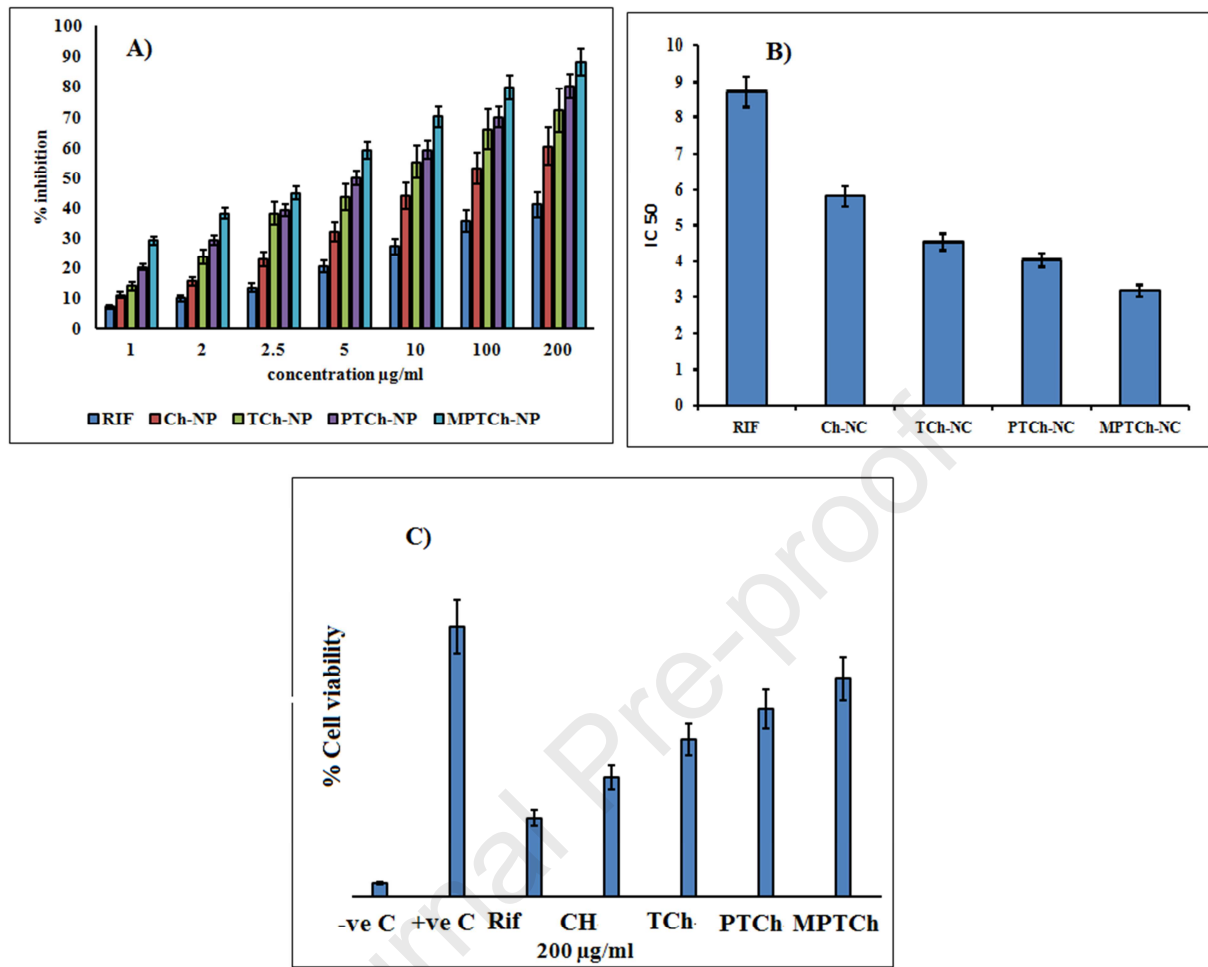
Figure 4
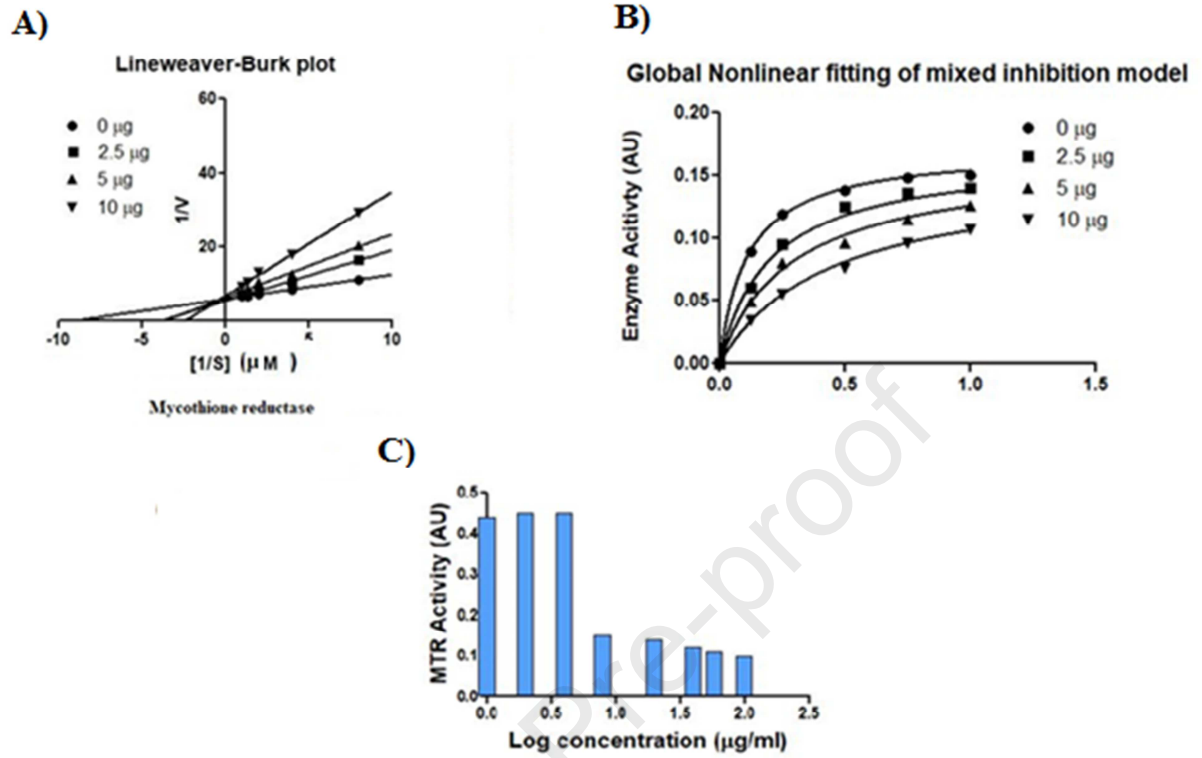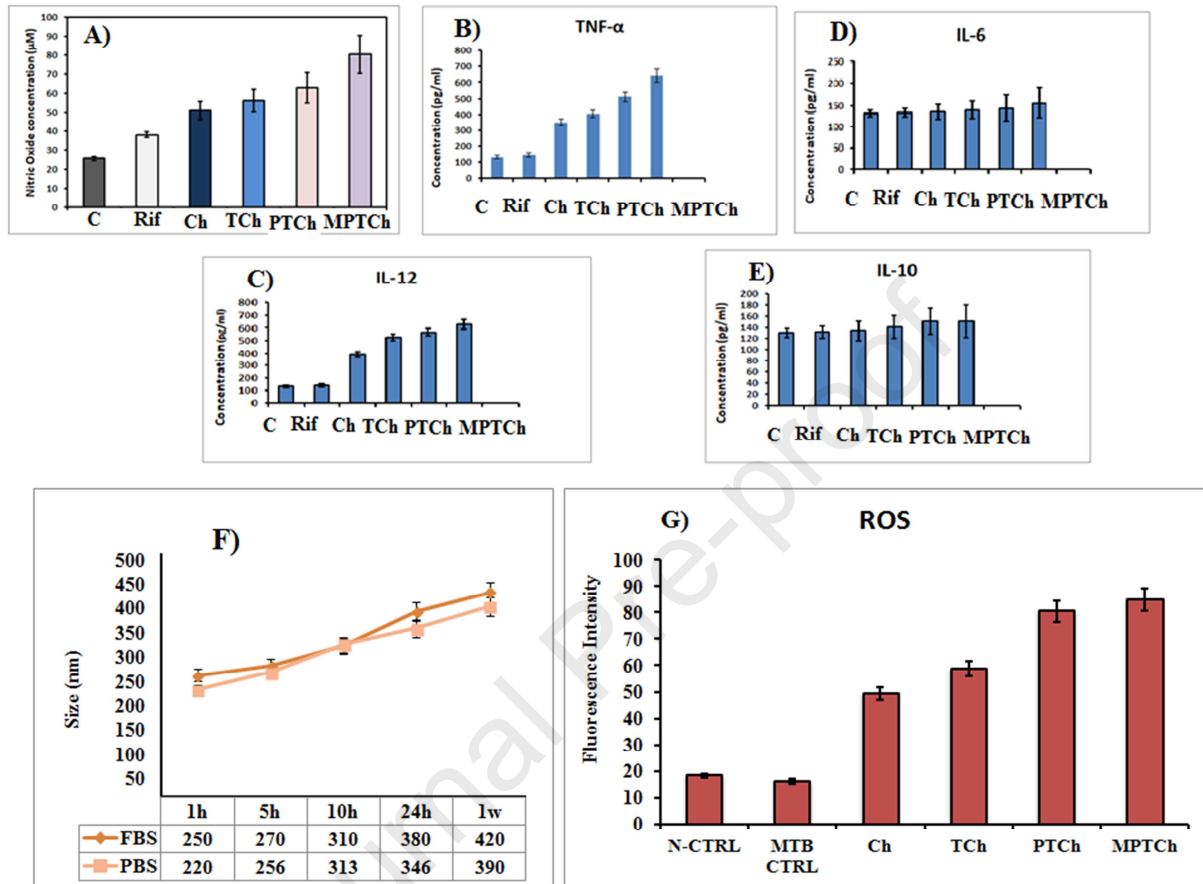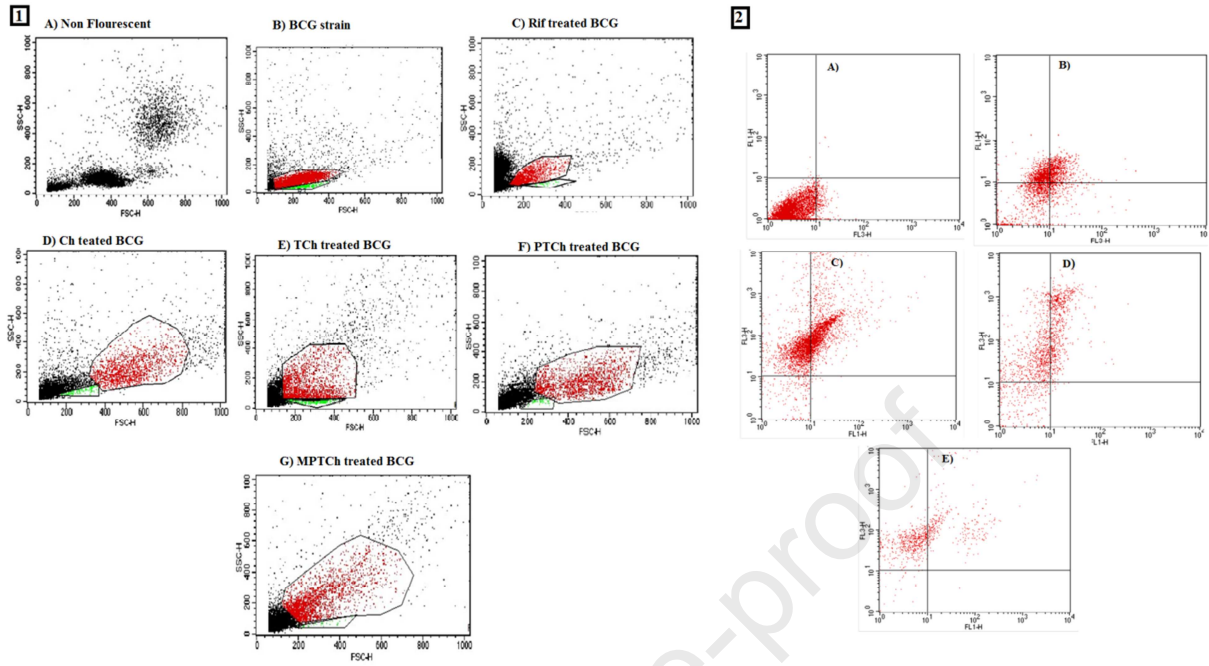
Figure 5

Figure 6

Figure 7

Figure 8

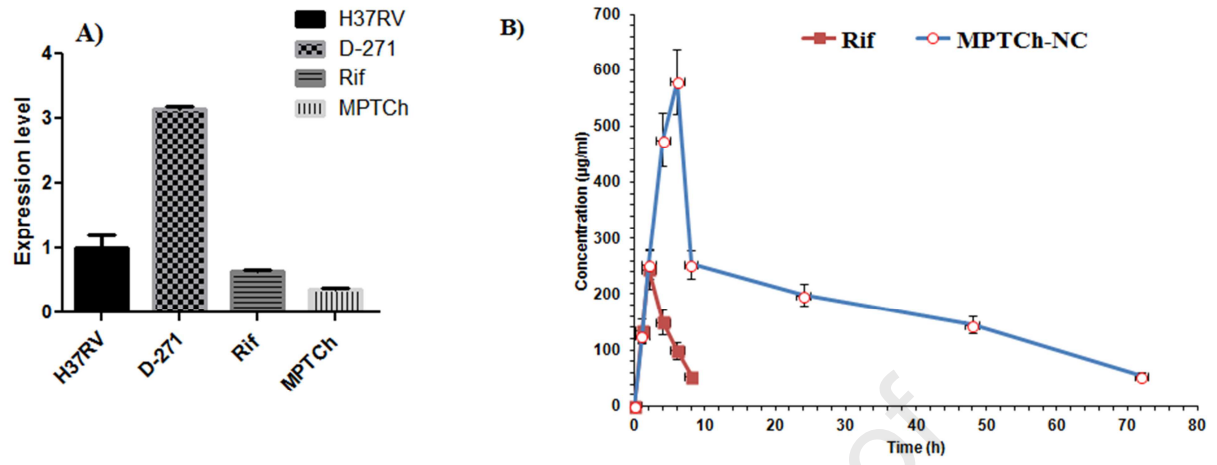**Declaration of interests**

☒ The authors declare that they have no known competing financial interests or personal relationships that could have appeared to influence the work reported in this paper.

☐The authors declare the following financial interests/personal relationships which may be considered as potential competing interests: